
Article:
Tindall, J orcid.org/0000-0002-2360-5761 and Haywood, A orcid.org/0000-0001-7008-0534 (2020) Modelling the mid-Pliocene warm period using HadGEM2. Global and Planetary Change, 186. 103110. ISSN 0921-8181

https://doi.org/10.1016/j.gloplacha.2019.103110

Modelling the mid-Pliocene Warm Period using HadGEM2.

Julia C. Tindall, Alan M. Haywood

School of Earth and Environment, University of Leeds, Leeds, LS2 9JT, UK

Abstract

Here, for the first time, we present simulations of mid-Pliocene climate using a UK IPCC AR5-class model (HadGEM2). The global annual mean surface air temperature increases by 3.4°C compared to the preindustrial control, with warming amplified towards the poles. The overall sensitivity of surface air temperature and polar amplification in response to the specification of the Pliocene boundary conditions is greater in HadGEM2 than in a previously utilised UK model (HadCM3). The simulated temperature anomaly is also at the upper range of that produced by the first phase of the Pliocene Model Intercomparison Project ensemble. Energy balance analysis indicates that the polar amplification of the mid-Pliocene warming in HadGEM2 is due to greenhouse gas emissivity changes and surface albedo changes. Approximately $5 \times 10^6 \text{km}^2$ of Arctic sea-ice is lost in the HadGEM2 Pliocene simulation and the global precipitation increases by 0.18mm/day, these anomalies are approximately twice as large as seen in HadCM3. HadGEM2 can retain a much larger amount of soil moisture than HadCM3, such that the amount of evaporation (and precipitation) over the land surface in the mid-Pliocene simulation is not as strongly constrained by water availability. These results highlight the importance of using more recently developed climate and Earth System Models to simulate the past. They further underline that our appreciation of Pliocene climate is model

*Corresponding author
Email address: earjcti@leeds.ac.uk (Julia C. Tindall)

dependant and ultimately limited by our physical understanding of the climate and the way this is represented in models.

Keywords: Pliocene, climate modelling, HadGEM2, hydrological cycle, polar amplification

1. Introduction

The mid-Pliocene Warm Period (mPWP; also referred to as the mid-Piacenzian Warm Period) is widely recognised as a geological example of a warmer world that, in fundamental ways, parallels climate model simulations of this century (Haywood et al., 2013). Recently Burke et al. (2018) assessed model simulations from six different geological timeperiods. They found that if the current path of rising CO_2 concentration in the atmosphere were continued, the mPWP was the most similar geological benchmark to global surface temperature predictions of 2030 CE. Continuing further on the current CO_2 concentration trajectory led to the emergence of a simulated Eocene-like pattern of surface temperatures as early as 2150 CE. Therefore, in the next 130 years the current pathway for CO_2 emission is likely to reverse a natural trend towards cooler surface temperatures that has taken 50 million years to accomplish. As such, the scientific community is placing ever greater emphasis on the study of warm climates in earth history using ensembles of climate and Earth System Models (Otto-Bliesner et al., 2017; Lunt et al., 2017; Haywood et al., 2016).

Numerical climate simulation of the mPWP have been carried out since the 1990's (Chandler et al., 1994; Sloan et al., 1996), and during the last 25 years has become a mainstream activity in palaeoclimatology. Within the UK Pliocene climate simulations have transitioned from atmosphere-only (Haywood et al., 2000), through atmosphere-slab ocean (Haywood et al., 2002) and fully coupled atmosphere-ocean models (Haywood and Valdes, 2004), to atmosphere-ocean models incorporating dynamic representation of global vegetation (Haywood and Valdes, 2006). The wider co-ordinated international community en-

gagement in simulating climates of the mPWP has been formalised through the creation of the Pliocene Model Intercomparison Project (PlioMIP) Phase 1 (PlioMIP1 Haywood et al., 2011) and Phase2 (PlioMIP2: Haywood et al., 2016).

Of the climate modelling studies carried out for the mPWP, it is important to recognise that many simulations have been run with climate models of IPCC AR3 and AR4 class. For example, the UK mPWP simulations have been run using HadCM3 (Hadley Centre Coupled Climate Model Version 3), a model that was released almost 20 years ago (Gordon et al., 2000) and used to produce future climate projections for the IPCC AR3 and AR4 (Solomon et al., 2007; Stocker et al., 2013). Although HadCM3 still performs very well in terms of its overall skill (Valdes et al., 2017), it is highly parametrized in terms of key atmosphere and oceanic processes, and some processes (e.g. aerosol/cloud climate feedbacks) are not resolved by the model at all.

Deficiencies in the details of the HadCM3 reproduction of mPWP climate have become more apparent since its first use (Haywood and Valdes, 2004). For example, Prescott et al. (2018) used HadCM3 with dynamic vegetation to explore the effect of strong interglacial orbital forcing on regional climate and seasonality during the mPWP. Over Eurasia there was insufficient precipitation and available soil moisture in order for the model to maintain the forests reconstructed from high resolution palaeobotanical records.

Here, for the first time, we employ an IPCC AR5-class Earth System Model, HadGEM2 (Hadley Centre Global Environmental Model version 2; The HadGEM2 Dev Team, 2011) to simulate the mPWP. In particular, we focus on the HadGEM2 simulation of critical features of the mPWP earth system, including the reproduction of large-scale climate features such as the meridional temperature gradient, the hydrological cycle, global energy balance, sea-ice and soil moisture content. We also use the model's outputs to produce revised simulations of global land cover that we compare to available synthesises of biome types based

on palaeobotanical data (Salzmann et al., 2008). Results will be compared to HadCM3 where appropriate and improvements in climate processes between the two models and their significance will be discussed.

2. Methods

2.1. Model description

2.1.1. HadGEM2

HadGEM2 can be thought of as a 'family' of models (The HadGEM2 Dev Team, 2011), which comprises a range of specific model configurations incorporating different levels of complexity, but with a common physical framework. The physical model configuration is derived from the HadGEM1 climate model (Johns et al., 2006) with a number of enhancements incorporated to improve model performance (Martin et al., 2006, 2010). A detailed description of the differences between the HadGEM1 model and the HadCM3 model is included in Johns et al. (2006) and Martin et al. (2006), and is summarised in the supplementary information.

The family of HadGEM2 model configurations range from an atmospheric only version (HadGEM2-A) to the full earth system version (HadGEM2-ES) which was used for CMIP5 (Collins et al., 2011). HadGEM2 has not been used extensively for paleoclimate studies. However HadGEM2-A, (with and without earth system components) has been used to investigate the last glacial maximum (Hopcroft et al., 2017; Hopcroft and Valdes, 2015).

Here we investigate the mPWP using the Atmosphere-Ocean configuration, HadGEM2-AO, but also incorporate dynamic vegetation. We do not use the ocean biogeochemistry and tropospheric chemistry components that are in the HadGEM2-ES configuration as these increase the cost of the model by a factor of 3 (The HadGEM2 Dev Team, 2011) making it infeasible for the multi-century

scale simulation required here. The HadGEM2 Dev Team (2011) showed consistency in the climate predictions between different HadGEM2 family members for the modern climate. However we note that there may be important feedbacks from the earth system components in the mPWP that we are not including here (Unger and Yue, 2014). Throughout this paper the HadGEM2 family member we use (HadGEM2-AO+dynamic vegetation) will simply be referred to as HadGEM2.

HadGEM2 has 38 atmospheric levels between the surface and 40km, with horizontal resolution of 1.875° longitude X 1.25° latitude. The atmospheric component uses the Arakawa-C grid horizontally with scalar variables such as temperature and density staggered from vector fields such as winds. The oceanic component is on a regular Arakawa-B grid, with longitudinal spacing of 1° everywhere, while latitudinal spacing is 1° polewards of 30°, which increases smoothly to 1/3° at the equator. There are 40 unevenly spaced vertical levels. Coupling between the ocean and atmosphere is on a daily timescale (Collins et al., 2011).

2.1.2. HadCM3

Although the purpose of this paper is to present results of the mPWP from the HadGEM2 model, results will be compared to one of its predecessors, the Hadley Centre General Circulation Model, HadCM3. This will allow continuity of mPWP modelling between model versions.

HadCM3 was originally described by Gordon et al. (2000) and Pope et al. (2000) and has been used in numerous scientific studies including the Intergovernmental Panel on Climate Change Fourth and Fifth Assessment Reports (Solomon et al., 2007; Stocker et al., 2013). Its atmospheric resolution is 3.75° longitude × 2.5° latitude × 19 vertical levels, which means there are 8 atmospheric gridboxes in HadGEM2 for each atmospheric gridbox in HadCM3. The oceanic resolution is also lower in HadCM3, especially near the equator, and is

1.25° longitude × 1.25° latitude × 20 unevenly spaced vertical levels. Coupling between the atmosphere and ocean is the same as HadGEM2 (once per day) as are the model timesteps (30 minutes for the atmosphere and 1 hour for ocean). The higher spatial resolution in HadGEM2 along with the increased complexity means that HadGEM2 is about 20 times slower to run, than HadCM3. However additional features can be captured in HadGEM2 (such as Indonesian Throughflow through the Makassar Strait; Johns et al., 2006).

The version of HadCM3 that we use in this paper has been described by Valdes et al. (2017) and includes the TRIFFID dynamic vegetation model (see section 2.1.3), and the MOSES2.1 surface exchange scheme. This is not the same as the HadCM3 version used for PlioMIP1, which used an earlier version of the surface exchange scheme (MOSES1) and fixed PRISM3 vegetation. There are some differences in predicted mPWP climate between the two versions of HadCM3 (e.g. Prescott et al., 2018; Tindall et al., 2016), hence the HadCM3 results presented here are not identical to those from PlioMIP1.

2.1.3. TRIFFID

In this study, both HadGEM2 and HadCM3 are interactively coupled to the dynamic vegetation model, TRIFFID (Top-down Representation of Interactive Foliage and Flora Including Dynamics; Cox, 2001). A detailed description of TRIFFID and how it is used within the Hadley Centre models is included in Valdes et al. (2017), however it is briefly summarised here for completeness. TRIFFID uses Lotka-Volterra competition equations to predict the properties and distribution of global vegetation. It dynamically attributes a fraction of the surface in each gridbox to bare soil and five plant functional types (PFT's: broadleaf tree, needleleaf tree, C3 grass, C4 grass and shrub). Three other surface types (land ice, urban and water) are fixed by model boundary conditions.

In both HadGEM2 and HadCM3, TRIFFID updates the vegetation once

every 10 days, using the 10 day average of the atmospheric fluxes to predict vegetation. However, because some vegetation types (in particular broadleaf trees) are very slow growing there is the possibility of running TRIFFID in spin up mode. This will use 5 years of climate fluxes to drive 50 years of TRIFFID vegetation growth, and will allow the vegetation to come into equilibrium with the climate more quickly. For the first 50 years of our simulations, TRIFFID was run in spinup mode, so that in these 50 years the vegetation component would have run for 500 years and forests would have been able to respond to the warmer model boundary conditions very quickly. For the remaining 450 years of the simulations, TRIFFID was continued in dynamic mode and was synchronously coupled to the climate. This latter portion of the simulation is of sufficient length that vegetation is expected to be in full equilibrium with the climate at the end of the simulation.

2.1.4. BIOME4

Many previous studies of the mPWP which have considered vegetation have used the BIOME4 model (e.g. Salzmann et al., 2008; Pound et al., 2014; Prescott et al., 2018). The BIOME4 model (Kaplan, 2001) is a mechanistic global vegetation model which predicts the distribution of 28 global biomes based on the monthly means of temperature, precipitation, cloudiness and absolute minimum temperature. Unlike TRIFFID, which allows multiple vegetation types to coexist within each gridbox, BIOME4 presents the biome that is dominant in each gridbox based on bioclimatic tolerances.

For consistency with previous work, and also to provide an alternative vegetation retrodiction to that of TRIFFID, we will also use the HadGEM2 climate data to drive BIOME4. It is noted that BIOME4 is not directly coupled to HadGEM2 and instead is run offline, driven by the HadGEM2 climate. This means that while the TRIFFID surface types will affect the climate in HadGEM2 (for example by modulating surface albedo), BIOME4 will not. Nonetheless

comparing and contrasting results between TRIFFID and BIOME4, and also comparing to paleodata (see section 5) will allow an assessment of the vegetation that could occur in the HadGEM2 mPWP climate.

2.2. Boundary conditions

HadGEM2 simulations have been set up for the preindustrial and the mPWP. The simulations were based on a modern HadGEM2-AO simulation that was altered by switching off the sulphur cycle, soot emissions and anthropogenic greenhouse gas emissions, and switching on dynamic vegetation. The preindustrial and mPWP simulations were then initialised at year 1859 and continued for 500 years. The oceanic state at the start of the simulations included an Atlantic Meridional Overturning Circulation (AMOC) with maximum strength of 18Sv. After 500 years this had reduced slightly to 16Sv for the mPWP experiment and 15Sv for the preindustrial experiment. This suggests little change in the strength of the AMOC between the mPWP and the preindustrial in HadGEM2 and is consistent with results from other models (Zhang et al., 2013).

The mPWP boundary conditions are derived mainly from PRISM3D (Dowsett et al., 2010); they are similar to those suggested for the 'alternate' experiment of PlioMIP1 (Haywood et al., 2011), and do not include changes in the ocean gateways that have been suggested for PlioMIP2 (Haywood et al., 2016). This means that the Bering Strait and the Canadian Arctic Archipelago both remain open. In polar regions, ice sheets and topography are PRISM3, however modern topography is used away from ice sheet regions to add more consistency with PRISM4 (Dowsett et al., 2016). Full PRISM4 boundary conditions are not used as these were not available when the simulations were started. The HadCM3 simulation that is used for comparison uses PRISM3 ice sheets and orography. Supplementary figure 1 shows the difference between the orography and ice sheets used to drive mPWP and preindustrial experiments for both HadGEM2 and HadCM3.

Consistent with PlioMIP1, CO_2 was set to 405ppmv while other trace gases were unchanged. The orbit for our simulations has been set to 3.205Ma, as this represents the Pliocene 'timeslice' discussed by Haywood et al. (2013), and was suggested as a target for data reconstruction. There are only very small differences between using the 3.205Ma orbit and a modern orbit (Hunter et al., 2019).

Initial conditions (e.g. deep soil temperature, soil moisture and snow cover) were all incorporated following Bragg et al. (2012) and were based on PRISM3. However these fields are all modified by the model and are expected to reach equilibrium with the modelled boundary conditions relatively early in the simulation. The climate at the end of the 500 year simulation will likely be independent of the initial deep soil temperature, soil moisture and snow cover chosen. Vegetation was initialised as preindustrial and TRIFFID was run in accelerated spinup mode for the first 50 years of the simulation (see section 2.1.3). This allows vegetation to reach quasi-equilibrium with the climate within the first 50 years of the simulations, and allows the vegetation to provide realistic climate feedbacks throughout the remaining 450 years.

To assess sensitivity to initial conditions we ran two mPWP simulations. The first is initialised directly from the 1859 climate with changes only to the boundary conditions, the second is also initialised from the preindustrial, but with 2°C added uniformly over the full area and depth of the ocean because the ocean was warmer during the mPWP (Dowsett et al., 2013).

2.3. Spinup

Due to the complexity and slow run time (< 2 model years per day) of the HadGEM2 model, the simulation length for the experiments has been limited to 500 years. Although this is in line with CMIP guidelines (Taylor et al., 2012), it is important to ensure that the mPWP climate in our simulation represents a spun-up climate. We consider the extent to which the global averaged sim-

ulations are in equilibrium by calculating the top of the atmosphere (TOA) radiative balance and by calculating the drift in globally averaged ocean and air temperatures. These are shown in Supplementary Table 1 and figure 1.

After 500 years the HadGEM2 preindustrial simulation has not reached full equilibrium. The TOA radiation balance is small but positive (0.44W/m^2) and is consistent with the value of 0.5W/m^2 cited by The HadGEM2 Dev Team (2011). There is also a small drift in ocean temperature of 0.03°C / century, however the globally averaged ocean surface temperature and surface air temperature are stable (figure 1). Imbalances and drifts in the mPWP experiments cannot be expected to be smaller than those in the preindustrial experiment, hence these values from the preindustrial provide a target value for the mPWP simulations. After 500 years the mPWP simulation that was initialised directly from the preindustrial simulation has a larger TOA radiation imbalance (0.82W/m^2) and ocean temperature drift (0.17°C / century) than the preindustrial, the ocean surface temperature and surface air temperature are also increasing; therefore this simulation is not close enough to equilibrium to provide meaningful results. Initialising the mPWP with an ocean 2°C warmer than preindustrial gives both a TOA radiation balance (0.47W/m^2) and ocean temperature drift (0.06°C / century) that is comparable to our preindustrial target, along with no clear drifts in the globally averaged surface temperatures. This implies that this simulation is sufficiently close to equilibrium to provide the HadGEM2 response to the mPWP boundary condition changes. Therefore, this paper will consider climate changes between the preindustrial and the mPWP simulation that was initialised from a 2°C warmer ocean. The latter will hereafter be referred to as the HadGEM2 mPWP simulation.

The HadCM3 preindustrial model has been run for tens of millennia, it has Top of the Atmosphere (TOA) radiation of -0.02W/m^2 and negligible ocean drift. A 2500-year mPWP simulation performed with HadCM3 (Tindall and Haywood, 2015) and initialised from preindustrial shows just how long a spinup

is needed to get the TOA radiation into complete balance. After 500 years of this simulation the TOA radiation is $0.37\mathrm{W/m^2}$, and while this had reduced to $0.32\mathrm{W/m^2}$ after 2500 years, this field is not fully in equilibrium in the mPWP simulation. However, since the drifts and imbalances in this simulation are comparable to HadGEM2, this HadCM3 simulation will be used for comparing climate results with HadGEM2.

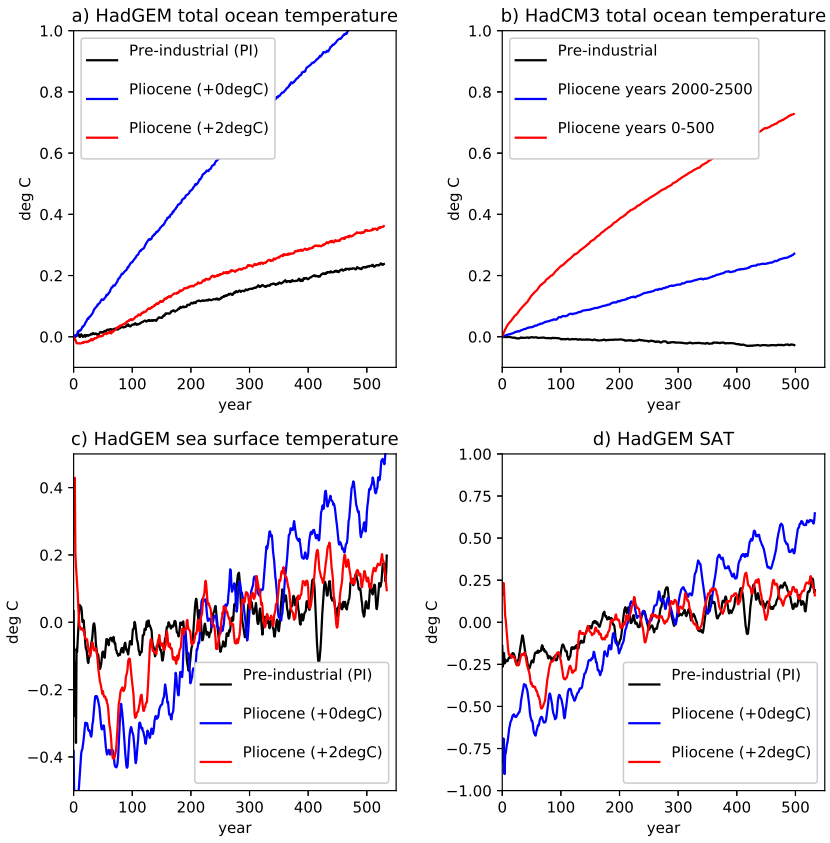

Figure 1: Globally averaged ocean temperature for HadGEM2 (a) and HadCM3 (b) averaged over the full depth of the ocean. In a) and b) the temperature at year 1 has been removed from each point. HadGEM2 sea surface temperature (c) and surface air temperature (d) throughout the simulation. c) and d) show a running 10 year mean for clarity, and the average throughout the simulation has been removed from each experiment. The HadGEM2 Pliocene experiment initialised from a 2°C warmer ocean has a very similar drift to preindustrial. Note also that the HadCM3 mPWP experiment is not fully spun up even after 2500 years.

3. Annual Mean climate in the mPWP

Figure 2a shows the HadGEM2 mPWP minus preindustrial surface air temperature (SAT) anomaly, averaged over the final 50 years of the simulation. The global mean anomaly is 3.4°C (towards the upper end of the PlioMIP1 models; table 1) and is greater over the land (4.2°C) than the ocean (3.0°C).

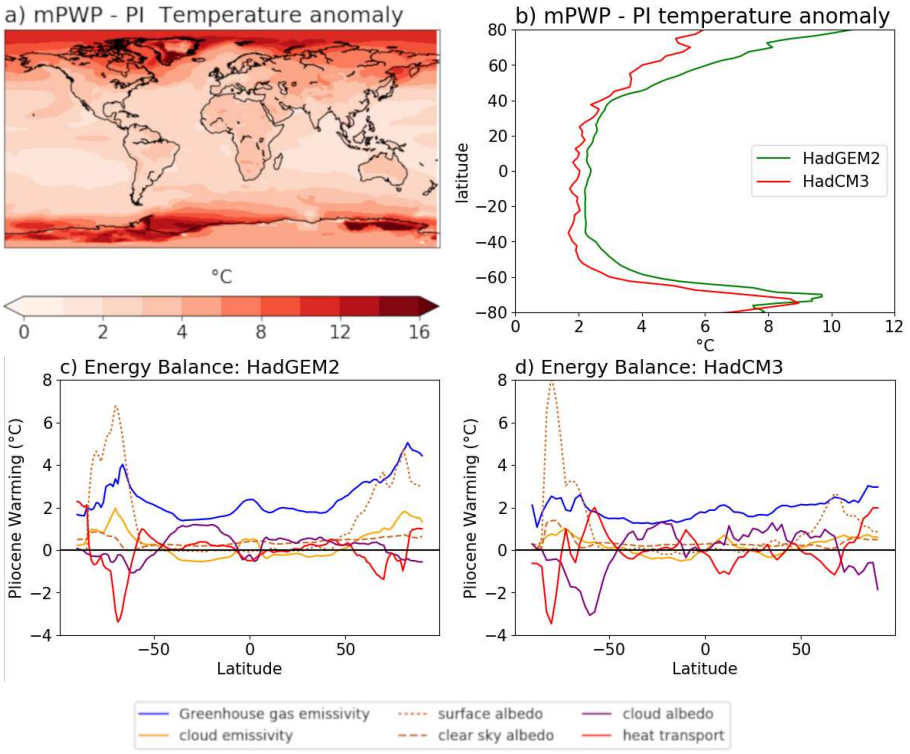

Figure 2: a) mPWP-preindustrial surface air temperature anomalies predicted from the final 50 years of the simulations, b) zonal mean temperature anomaly from HadGEM2 and HadCM3, c) and d) Energy balance analysis showing the cause of the zonal mean warming at each latitude for HadGEM2 and HadCM3.

MODEL	SEASON	Surface Air Temperature anomalies (°C)					Precipitation anomalies mm/day (percentage change)		
		Global	Land	Sea	60°N-90°N (75°N-90°N)	60°S-90°S (75°S-90°S)	Global	Land	Sea
PlioMIP1	ANN	1.8-3.6	2.1-5.1	1.5-3.2			0.09-0.18	-0.1-0.27	0.08-0.26
HadGEM2	ANN	3.4	4.2	3.0	8.0 (10.1)	7.1 (7.3)	0.18 (6)	0.15 (6)	0.20 (6)
HadCM3	ANN	2.6	3.9	2.1	4.8 (5.6)	5.5 (6.3)	0.09 (3)	0.04 (2)	0.11 (3)
HadGEM2	DJF	3.4	4.3	2.9	10.1 (14.0)	5.8 (7.1)	0.19 (6)	0.09 (4)	0.24 (7)
	MAM	3.4	4.6	2.9	8.9 (9.2)	7.2 (8.4)	0.18 (6)	0.21 (9)	0.16 (5)
	JJA	3.4	4.1	3.0	4.6 (3.3)	8.4 (7.0)	0.18 (6)	0.21 (8)	0.16 (5)
	SON	3.4	3.8	3.2	8.0 (13.2)	7.0 (6.3)	0.20 (7)	0.07 (3)	0.27 (8)
HadCM3	DJF	2.3	3.5	1.8	5.5 (7.2)	4.6 (7.6)	0.10 (3)	-0.02 (-1)	0.14 (4)
	MAM	2.5	4.0	1.9	4.9 (4.9)	5.1 (6.3)	0.08 (3)	0.06 (3)	0.09 (3)
	JJA	2.9	4.6	2.2	4.0 (2.1)	6.2 (5.1)	0.06 (2)	0.09 (4)	0.05 (2)
	SON	2.6	3.4	2.2	4.8 (8.3)	5.9 (6.4)	0.12 (4)	-0.01 (0)	0.17 (5)

Table 1: Global mean temperature and precipitation anomalies from HadGEM2 and HadCM3.

In agreement with other simulations of the mPWP, HadGEM2 shows polar amplification of temperature change. (Compared with HadCM3 on figure 2b and in table 1). In HadGEM2 the polar amplification is larger in the Northern Hemisphere than the Southern Hemisphere which is opposite to what is shown by HadCM3. Figures 2c and 2d show the mPWP warming decomposed into energy balance contributions for HadGEM2 and HadCM3 respectively (calculated following Hill (2015) with albedo improvements suggested by Feng et al. (2017) and Taylor et al. (2007)). It is seen that the energy balance is quite different between the two models, particularly at high latitudes. This can be seen more clearly on supplementary figure 2 which shows each energy balance component individually for both models.

The 3.4°C global mean HadGEM2 SAT anomaly can be attributed to greenhouse gas emissivity changes (2.1°C), surface albedo changes (0.6°C) clear sky albedo changes (0.3°C) and cloud albedo changes (0.3°C), along with minor contributions from cloud emissivity and topography. Heat transport (presented as the sum of atmospheric and oceanic heat transport) changes the distribution of the latitudinal warming, with a reduction in poleward heat transport poleward of 50° slightly offsetting some of the high latitude warming attributed to surface albedo changes. The polar amplification of HadGEM2 warming is predominantly due to surface albedo changes and polar amplification of the effects of greenhouse gas emissivity (figure 2c and supplementary figure 2), which is likely due to increases in atmospheric water vapour at high latitudes (Hill, 2015). This polar amplification of greenhouse gas emissivity and surface albedo is not seen to the same extent in HadCM3 (supplementary figure 2); here temperature change attributable to greenhouse gas emissivity varies little with latitude. There are also smaller changes related to surface albedo because there is less sea ice loss in HadCM3 (see section 4). Results from figure 2 appear qualitatively consistent with other PlioMIP1 models (Hill, 2015). The relative importance of different energy balance terms poleward of 55°N also agrees with the CCSM4 model (Feng et al., 2017). However, they are approximately a factor of 2 greater

in HadGEM2 than in CCSM4, leading to greater northern hemisphere polar amplification overall.

Figure 3a shows the mPWP - preindustrial precipitation anomaly from HadGEM2 (with global averages shown in table 1). In order that this figure is not dominated by regions of high precipitation, it has been presented as a percentage change from preindustrial. It is seen that precipitation is higher in the mPWP simulation throughout the mid and high latitudes. In the tropics some regions show reduced precipitation: at the locations of the southern subtropical highs, over southern Africa, Australia, the Sahara and the Middle East. The drying of the Sahara and the Middle East does not occur in the ensemble mean from PlioMIP1 (Haywood et al., 2013), or the HadCM3-MOSES1 contribution to PlioMIP1 (Bragg et al., 2012) because the PRISM3 vegetation reconstruction (Salzmann et al., 2008) incorporated into PlioMIP1 shows denser vegetation in these regions than the TRIFFID DGVM is able to maintain (Prescott et al., 2018), and this denser vegetation feeds back onto a wetter mPWP climate. In contrast, the HadCM3-MOSES2 simulation which has dynamic vegetation (figure 3b), enhances the drying relative to HadGEM2. With dynamic vegetation the increase in land precipitation in HadGEM2 is over 3 times larger than that in HadCM3 (see also table 1).

Figures 3c and 3d shows the percentage change in evaporation between the preindustrial and the mPWP, for HadGEM2 and HadCM3 respectively. Over land there is strong coherence between precipitation and evaporation because precipitation determines local water availability for evaporation. However the two models strongly disagree over land evaporation changes: globally averaged mPWP land evaporation was 0.11mm/day higher than preindustrial in HadGEM2, but 0.06mm/day lower than preindustrial in HadCM3.

Evaporation over land is limited by moisture availability. The difference in available soil moisture between the mPWP and the preindustrial is shown

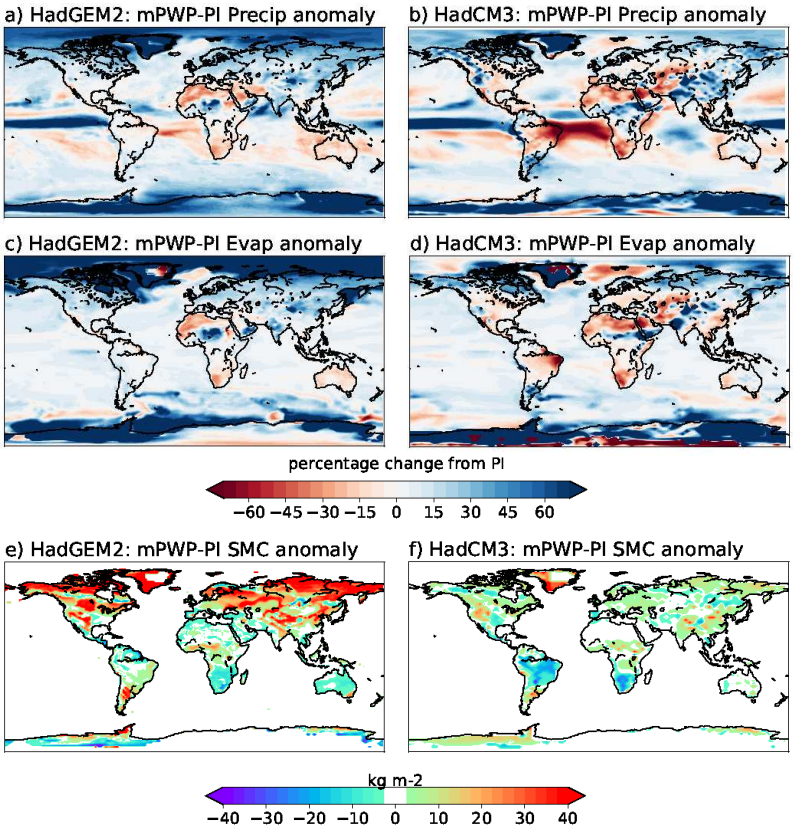

Figure 3: mPWP-preindustrial precipitation, evaporation and soil moisture anomalies predicted from final 50 years of the simulations for HadGEM2 (left) and HadCM3 (right).

in figures 3e and 3f. It is seen that there is a large increase in this field in HadGEM2, particularly at high latitudes, while there are relatively minor changes in HadCM3. There are 3 main reasons for the differences in available soil moisture between the two models. Firstly the warmer mPWP temperatures in HadGEM2 means that a lower fraction of the soil moisture is frozen, secondly there have been changes to the land surface hydrology scheme in HadGEM2 (Martin et al., 2010, Table A2), many of which are designed to improve soil water and hydrological budgets and finally there is an hydrological feedback,

with much of the additional evaporation returning to the land surface via precipitation. The large increase in available soil moisture in HadGEM2 (relative to HadCM3) means that land evaporation is more strongly related to the temperature increase in HadGEM2 and less constrained by water availability than in HadCM3.

Soil moisture does not effect ocean precipitation or evaporation. Therefore precipitation and evaporations over oceans is expected to be more consistent between the models. This is indeed the case, table 1 shows that the land precipitation anomaly in HadCM3 is only 27% of that in HadGEM2, while the ocean precipitation anomaly in HadCM3 is 55% of that in HadGEM2. Over oceans evaporation is predominantly determined by temperature and is greater in both models, but particularly in the high latitude regions of HadGEM2 where the largest temperature changes occur.

Precipitation changes in HadGEM2 are within the range obtained from PlioMIP1 models (see table 1). The globally averaged precipitation anomaly of 0.18mm/day is at the upper range of the PLIOMIP1 ensemble (0.09-0.18 mm/day), while the HadCM3 precipitation anomaly is at the lower end (0.09mm/day). It is noteworthy that the globally averaged precipitation increase in PlioMIP1 models is not evenly distributed throughout the range, and a number of models (FGOALS2 (Zheng et al., 2013), COSMOS (Stepanek and Lohmann, 2012), GISS2 (Chandler et al., 2013) and MIROC4 (Chan et al., 2011)) are also near the upper end of the PlioMIP1 range. Figures 3a and 3b, show that the precipitation anomaly increases towards the poles particularly in HadGEM2. The increase in precipitation is larger in HadGEM2 than HadCM3 partly because polar amplification is higher. The divergence between the two models increases with latitude such that the precipitation anomaly is twice as large in HadGEM2 than in HadCM3 near the north pole.

4. Seasonal Climate

4.1. Seasonal Temperature and Polar Amplification

Figure 4(a-d) and table 1 shows the seasonal SAT anomaly between the mPWP and the preindustrial as simulated by HadGEM2. (Supplementary figure 3 shows the SAT anomaly for HadCM3). In HadGEM2 we see that the annual mean polar amplification is mainly due to changes in the winter season (although spring and autumn also play a role). In HadCM3 the seasonal patterns are similar; however the winter high latitude warming is much less pronounced.

Arctic polar amplification is expected in a warming climate and has occurred in recent decades. Screen and Simmonds (2010) considered the causes of recent Arctic amplification, and found the Arctic warming was predominantly due to changes in albedo consistent with Arctic sea ice loss. Consistent with our mPWP modelling results (figure 4) Screen and Simmonds (2010) showed that ERA-Interim temperature trends over the Arctic are largest during DJF and SON and smallest in JJA. However, figure 2 suggests that polar amplification of greenhouse gas contribution was also a strong contributor to the mPWP warming, which was not seen in the modern attribution.

Figure 4e shows the areal extent of the preindustrial Arctic sea ice (blue) and the mPWP Arctic sea ice (red) over the year. The solid lines show results from HadGEM2 while the dotted lines show the results from HadCM3. The sea ice component of HadGEM2 is more complex than HadCM3, as components of the CICE (Hunke and Lipscomb, 2004) model have been incorporated and leads to a more realistic sea ice distribution for the modern climate (Johns et al., 2006).

All seasons show a substantial reduction in Arctic sea ice in the mPWP. In HadGEM2 the reduction in sea ice is approximately 5,000,000 km^2 and this is relatively constant throughout the year. This reduction in sea ice is sufficient

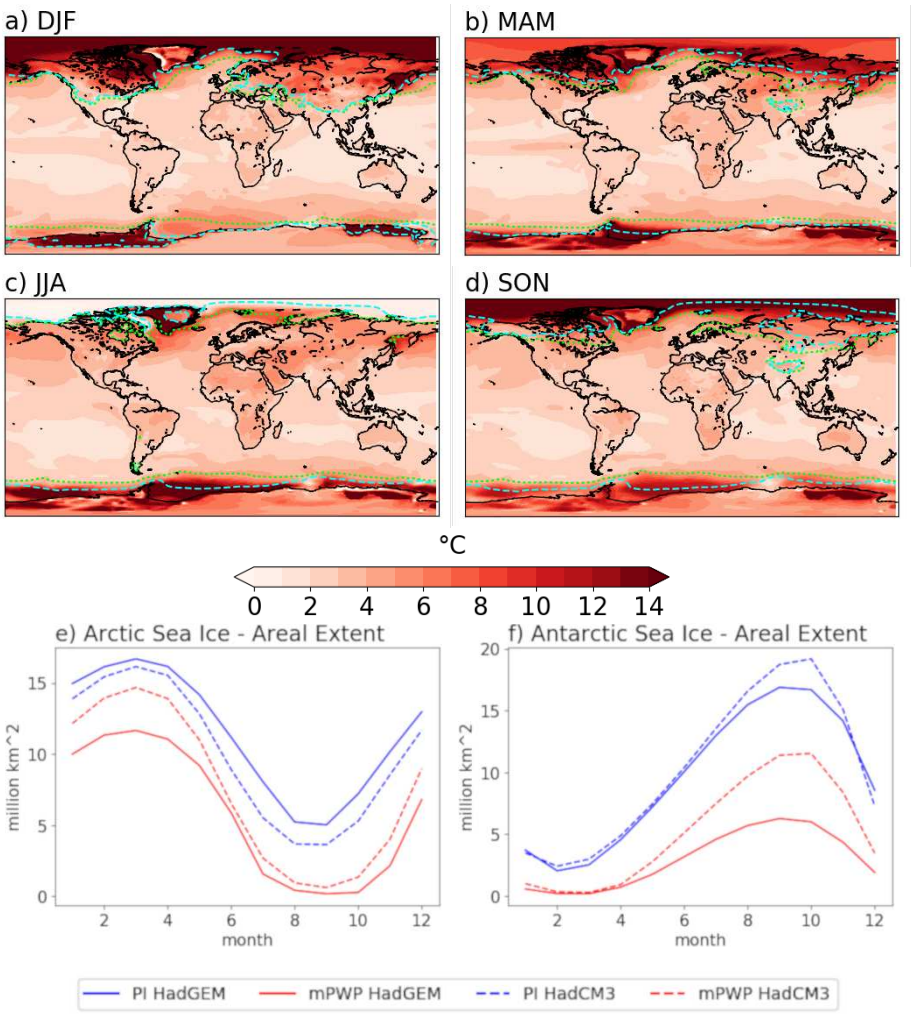

Figure 4: (a-d) mPWP-preindustrial SAT anomalies for each season. The blue and green dotted lines show the 0°C isotherm for the mPWP and PI respectively. (e-f) shows the areal extent of sea ice for the Arctic and Antarctica, by month, for HadGEM2 (solid) and HadCM3 (dashed)

that the Arctic is almost ice free in September, while the decline in ice volume to its annual minimum is steeper and recovery is slower than in the preindustrial. HadCM3 shows a smaller reduction in sea ice particularly in the winter and is

related to the lower polar amplification of temperature in HadCM3.

The areal extent of sea ice around Antarctica is shown in figure 4f. Again, a dramatic loss of sea ice is seen throughout the year, however HadGEM2 sea ice loss is strongest in the winter season. Indeed, in the austral winter, 2/3 of Antarctic sea ice is lost in HadGEM2, compared to only 1/3 of Arctic sea ice loss in the boreal winter. In the Southern Ocean near Antarctica the greatest warming occurs in the austral winter (JJA), highlighting the positive feedback of warmer temperatures preventing sea ice from forming, reducing the albedo and warming the oceans further. In HadCM3 this feedback loop is not as strong with the result that the mPWP ocean temperatures are not as high near Antarctica and sea ice loss is not as great.

4.2. Seasonal Precipitation at high latitudes

Figure 5 shows the seasonal precipitation and evaporation anomaly between the mPWP and the preindustrial in the Northern Hemisphere. Although precipitation has increased throughout the NH, the increase does vary with season. For example, the increase over Western Europe is largest in DJF while the increase over North Eastern Europe, Northern Canada and Alaska is largest in MAM. It is seen that high latitude land evaporation increases the most in MAM (and JJA) such that recycling can explain most of the precipitation increase over land in these seasons. In DJF, land evaporation changes little and the additional precipitation is sourced from the oceans. Here evaporation increases most strongly in the Atlantic sector of the Arctic Ocean, which showed much less sea ice in the mPWP (supplementary figure 4). There is a relationship between the degree of warming and the amount of evaporation both regionally and seasonally, particularly when evaporation is calculated as a 'percentage change' (not shown). In HadCM3 (supplementary figures 3 and 6) the seasonal and regional coherence between increased temperature and increased land evaporation are not apparent. For example, in JJA there is substantial warming over large continental

areas which show a decrease in evaporation. This is due to there being less available soil moisture for evaporation in HadCM3.

The precipitation anomaly between the mPWP and the preindustrial appears as a change in rainfall (figure 6 - HadGEM2, and supplementary figure 7 HadCM3). In HadGEM2, and to a lesser extent in HadCM3, there is a conversion from snow to rain such that there was less snowfall over most regions in the mPWP. The exception to this is the DJF season, where snowfall increases over large parts of Eurasia and North America. In DJF these regions are subzero and the 0°C isotherm (figure 4) does not change substantially between the two climates, so that the enhanced precipitation must fall as snow. In MAM the location of the 0°C isotherm changes substantially over land leading to a large conversion from snow to rain over the land surface.

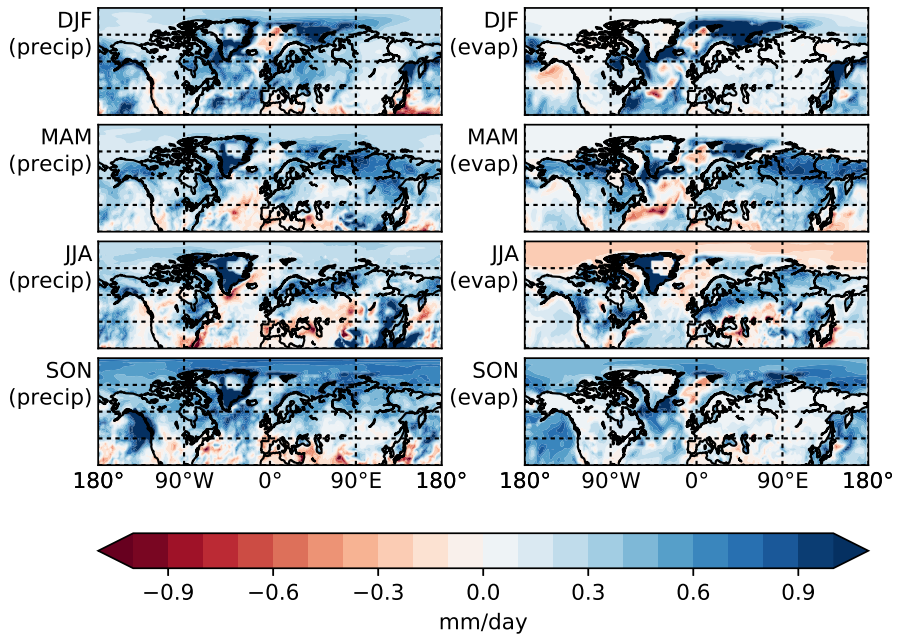

Figure 5: The HadGEM2 mPWP minus preindustrial anomaly for precipitation (left) and evaporation(right) over the NH for each season.

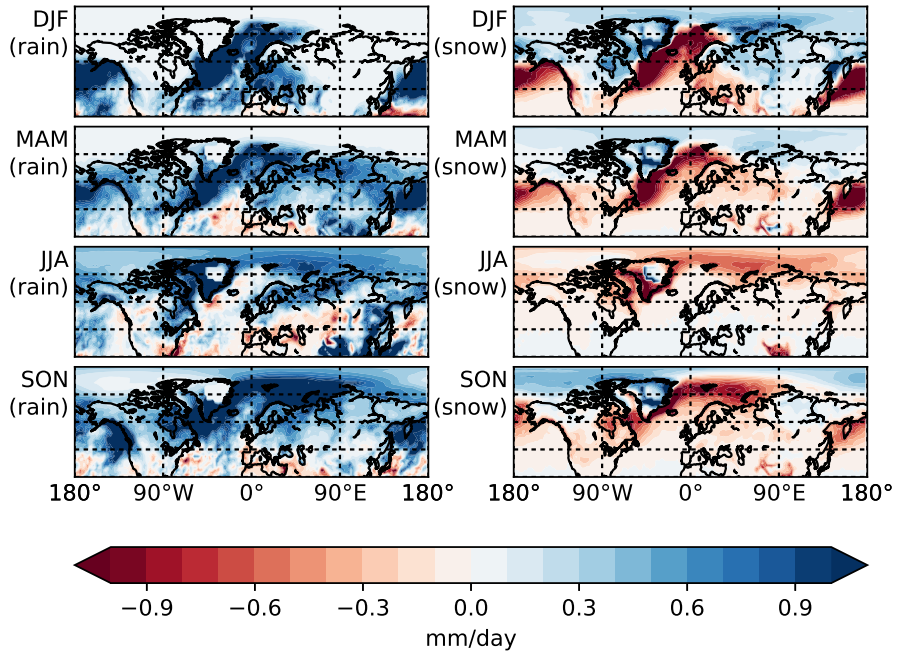

Figure 6: The HadGEM2 mPWP minus preindustrial anomaly for rain (left) and snow (right) over the NH for each season.

4.3. Seasonal surface albedo and ground cover

The rise in high latitude temperatures and the northward movement of the 0°C isotherm reduces the proportion of high latitude soil moisture that is frozen. Figure 7(left) shows the regions where the proportion of ground that is frozen exceeds 0.2 for the preindustrial (green contour) and the mPWP (red contour). Also shown is the fraction of HadGEM2 soil moisture that changes from frozen to unfrozen between the PI and the mPWP. In JJA frozen soil moisture fraction exceeding 0.2 has shifted to the very edge of the northern hemisphere continents in the mPWP and there is a large reduction of permafrost. In other seasons there is also a substantial reduction in the proportion of frozen soil moisture, with the largest change between the two climates occurring in MAM, where the shift in the 0°C isotherm is most apparent over land.

Figure 7 (right) shows the change in surface albedo (between the mPWP and the PI) for each season. Note that over land the albedo changes have been multiplied by a factor of 10, because sea ice changes dominate albedo changes, and because the specific heat capacity of the ocean is much larger than that of land. A fall in the albedo causes a significant proportion of the mPWP warming (figure 2). Over land the albedo changes are strongest in MAM due to the loss of snowfall and frozen ground, while over the oceans the albedo changes highlight the regions where sea ice has been lost (supplementary figure 4) and varies seasonally.

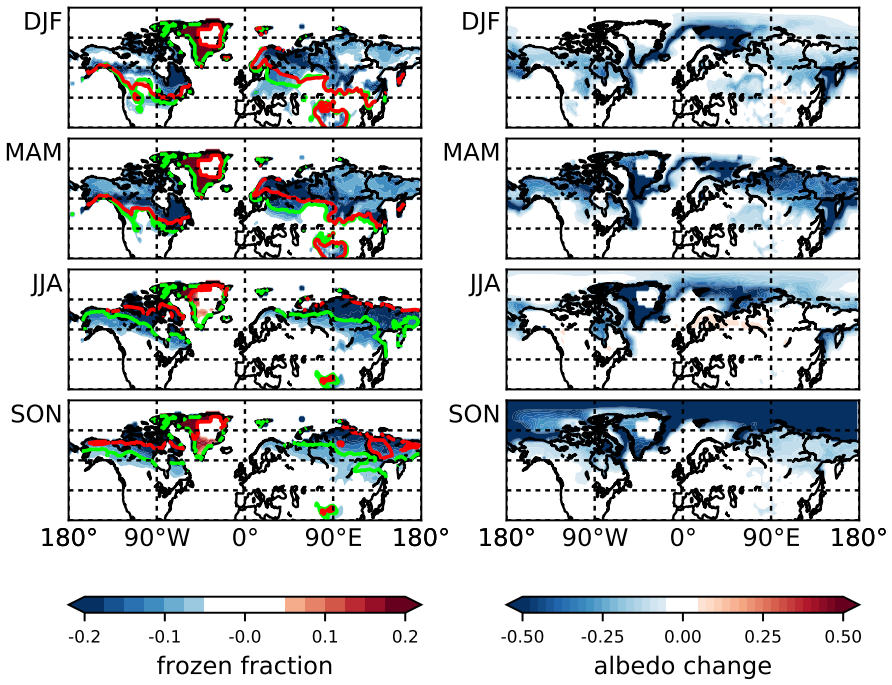

Figure 7: Left: Change in the fraction of soil moisture that is frozen between the mPWP and the PI, the contours highlight the regions where the frozen fraction of soil moisture exceeds 0.2 for the preindustrial (green) and the mPWP (red). Right: Change in the albedo between the mPWP and the PI, due to sea ice loss and changes in snow cover. Note that over land the albedo changes have been multiplied by a factor of 10.

4.4. ITCZ and tropical precipitation

Figure 3a shows that one of the most notable changes between mPWP and preindustrial precipitation is in the tropics and is related to the Intertropical Convergence Zone (ITCZ.) Tropical precipitation changes are in broad agreement with PlioMIP1 models (Corvec and Fletcher, 2017), with HadGEM2 and PlioMIP1 models showing an increase in land precipitation in a band covering the Sahel, the Southern Part of Arabia and India. They also see reduced rainfall over Southern Africa, central America and Eastern Brazil. The HadGEM2 ocean response is also in broad agreement with other models which show more rainfall in the Pacific ITCZ and a drier South Atlantic.

Figure 8 shows seasonal changes in tropical precipitation between the mPWP and the preindustrial (left) and also the seasonal zonal mean precipitation (right). There is a slight increase of ITCZ precipitation in all seasons, and overall precipitation in the ITCZ region has increased by about 5% relative to the preindustrial. The shape of the zonal mean precipitation is similar between the mPWP and the preindustrial, implying that the different climate is not altering the zonal-mean ITCZ position substantially. Despite this the anomaly plots (figure 8 - left) suggest that the location and intensity of the ITCZ changes on a regional basis. For example, in the Pacific sector there appears to be a southward shift of ITCZ rainfall in DJF/MAM and a northward shift in SON. In the Atlantic sector the ITCZ shifts southwards although there is a slight northward shift in JJA along with a slight enhancement of the West African Monsoon. The Indian Ocean ITCZ also moves northwards throughout the year, but particularly in the summer where the Indian Monsoon is enhanced.

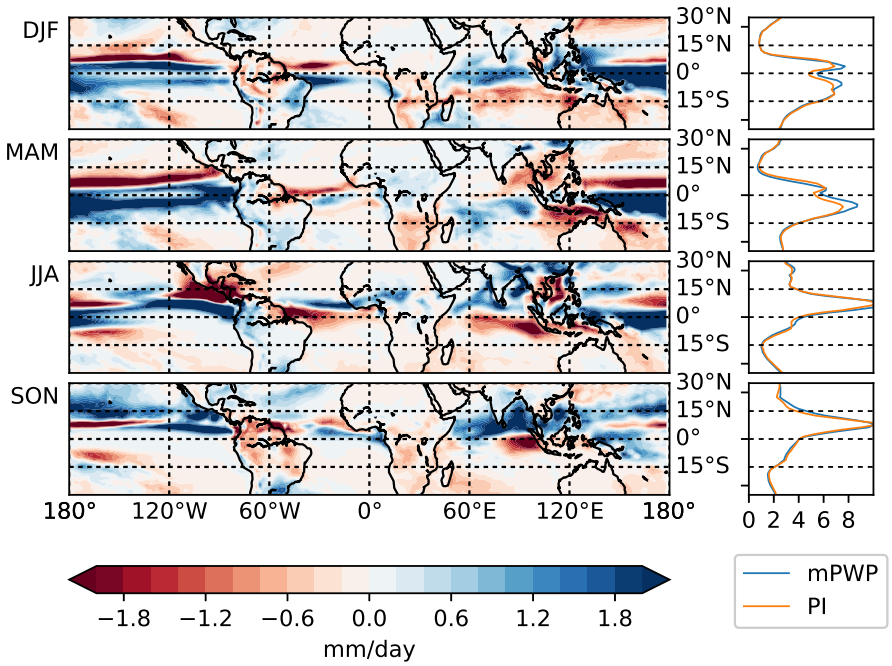

Figure 8: Maps (left) show the difference between mPWP precipitation and pre-industrial precipitation in the tropics for each season. Plots (right) show the total zonal tropical precipitation for the mPWP and the preindustrial.

5. Vegetation changes

The substantial temperature and precipitation changes between the mPWP and the PI, along with the increased CO_2 will affect vegetation. Two retrodictions of mPWP vegetation will now be considered. Firstly results from the coupled dynamic global vegetation model, TRIFFID, will be shown and secondly the HadGEM2 climate will be used to drive the BIOME4 model (Kaplan, 2001) in order to provide an alternative viewpoint of mPWP vegetation.

The plant functional types predicted by TRIFFID for the preindustrial and the mPWP are shown in figure 9 for HadGEM2 (and supplementary figure 8 for HadCM3). For simplicity shrubs, C3 grasses and C4 grasses have all been combined into a 'grasses' panel. Hopcroft and Valdes (2015) suggested that for the LGM climate some changes to the vegetation parameters in HadGEM2 were required to obtain a satisfactory vegetation distribution, however sensitivity tests (not shown) suggest that for the warm climate of the mPWP these parameter changes do not lead to substantially different results, hence the standard parameters have been used here.

HadGEM2 shows a drastic change in predicted vegetation between the two climates with the broadleaf trees in the NH latitudes showing the most remarkable change. Broadleaf trees were present in the NH in the PI simulation, but at relatively low concentrations. However, in the mPWP simulation, the increased temperature, increased precipitation, reduction in frozen soil and increase in CO_2 allows large parts of North America and Eurasia to support broadleaf trees. The increase in broadleaf trees is partly at the expense of needleleaf trees, and partly at the expense of grasses and shrubs. The NH grass and shrubland that was seen in the preindustrial has become relatively rare in the mPWP and has retreated into the very high latitudes that were previously barren and unable to support vegetation. The same general patterns are also seen in HadCM3 (supplementary figure 8 and Prescott et al., 2018) but to a much lower extent.

HadGEM2 and HadCM3 show general agreement in the direction of change, but not in magnitude, with HadGEM2 being much more sensitive.

Figure 10 shows the biome distribution obtained by using HadGEM2 outputs to drive the BIOME4 model for the preindustrial (left) and the mPWP (right). Results from BIOME4 are less dramatic than from TRIFFID, although general features are reasonably consistent. Like TRIFFID, BIOME4 shows a general increase in tropical forests, particularly in South America and East Asia. However, while Central Africa barely changed between the PI and the mPWP in TRIFFID, BIOME4 showed a reduction in forests along with an expansion of Savannah. The expansion of NH broadleaf trees at the mPWP (seen in TRIFFID) is also seen in BIOME4 (albeit to a lesser extent) and occurs across North America and Western Europe.

Over central Eurasia, BIOME4 maintains a larger proportion of grassland in the mPWP than TRIFFID, however the vegetation occurs further northward at the mPWP in both BIOME4 and TRIFFID. In agreement with TRIFFID, BIOME4 replaces the preindustrial shrub tundra at high latitudes with taiga/forest in the mPWP. Both TRIFFID and BIOME4 show similar patterns of desert/bare soil for the two climates, suggesting that the HadGEM2 climate cannot change the desert area substantially for these boundary conditions.

The PRISM3 vegetation reconstruction (Salzmann et al., 2008) includes data from 3.6-2.6Ma, and will therefore span a range of different Pliocene climates including glacials (e.g. the M2; Dolan et al., 2015) and interglacials with different orbital configurations. Although many data sites now include two vegetation reconstruction, one for a cold/dry climate and one for a warm/wet climate (Salzmann et al., 2013) the data does not claim to represent the 3.205Ma mPWP timeslice that we model here. Despite this caveat the northward shift of mid-high latitude vegetation zones in the mPWP simulation appears in good agreement with the data. In the tropics data suggests expanded tropical savannah

and forests at the expense of desert (Salzmann et al., 2008, 2013). This is seen to some extent in figure 10 by an expansion of forests over South Africa and South East Asia which are in good agreement with data, however deserts do not reduce significantly in the mPWP whether vegetation is simulated using either TRIFFID or BIOME4. Across central and Northern Eurasia the data suggests mainly forests/woodland and although data is limited in central Asia, it does not suggest the large expanse of grassland predicted by BIOME4. The TRIFFID retrodiction, suggesting mPWP forests in this region is in better agreement with the data.

HadGEM2 does not replicate the forests over Australia or the reduction in the extent of the Sahara Desert that the data implies. This is because the precipitation (figure 3) does not increase sufficiently in these regions to support vegetation growth. It is unclear whether this model-data disagreement is due to modelling issues (e.g. boundary conditions, model parametrisations) or whether it could be resolved by modelling a different mPWP timeslice. The HadCM3 modelling study of Prescott et al. (2018) showed that other mPWP interglacials (namely G17, K1 and KM3) had more rainfall over Australia and the Sahara than the timeslice considered here (KM5c). These other interglacials studies with HadCM3, all showed a slight reduction of tropical desert relative to KM5c, although in none of the interglacials was the reduction in desert as large as suggested by observations. However, this paper has consistently shown that HadCM3 does not appear to be as sensitive as HadGEM2, so perhaps the small reduction in desert that was simulated with HadCM3 would be enhanced if the HadGEM2 model were used and would provide better agreement with data.

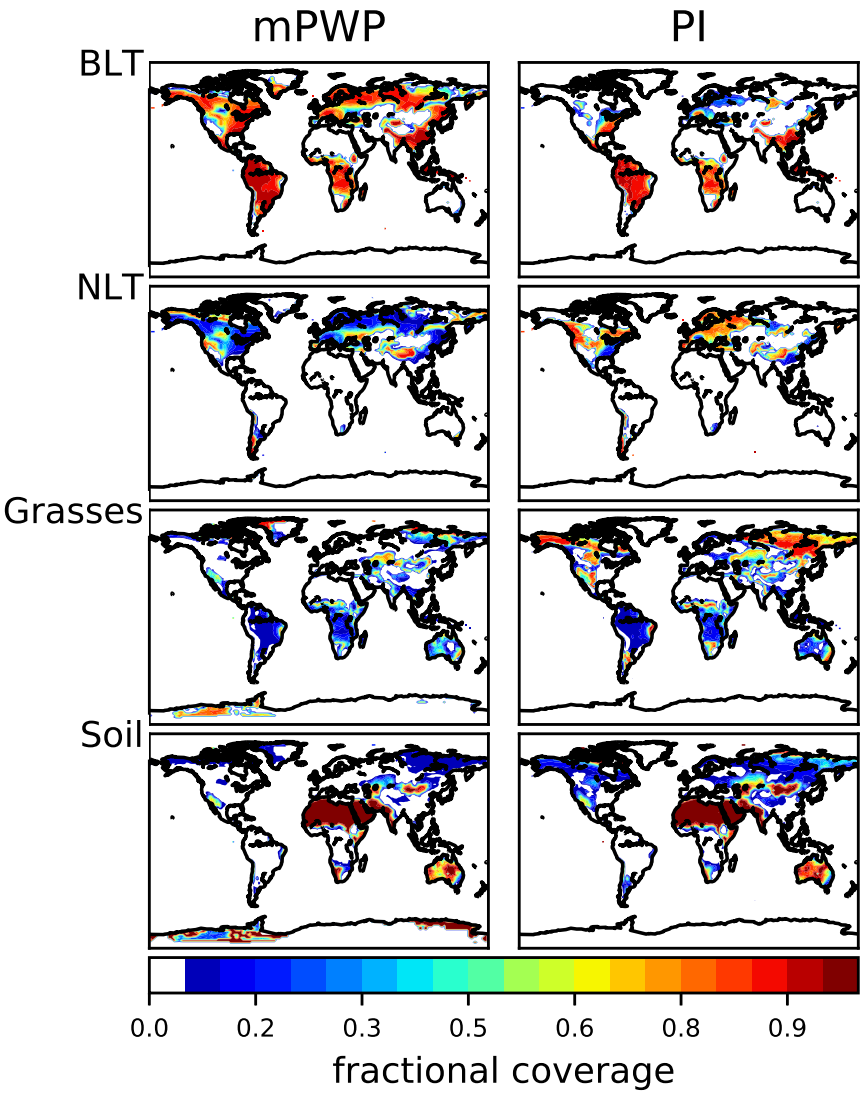

Figure 9: Shows the vegetation fraction dynamically attributed to each plant functional type (PFT) by TRIFFID in HadGEM2 for the mPWP (left) and the preindustrial (right). The PFT's are: BLT - broadleaf trees, NLT - needleleaf trees, Grasses - C3 grasses + C4 grasses + shrubs.

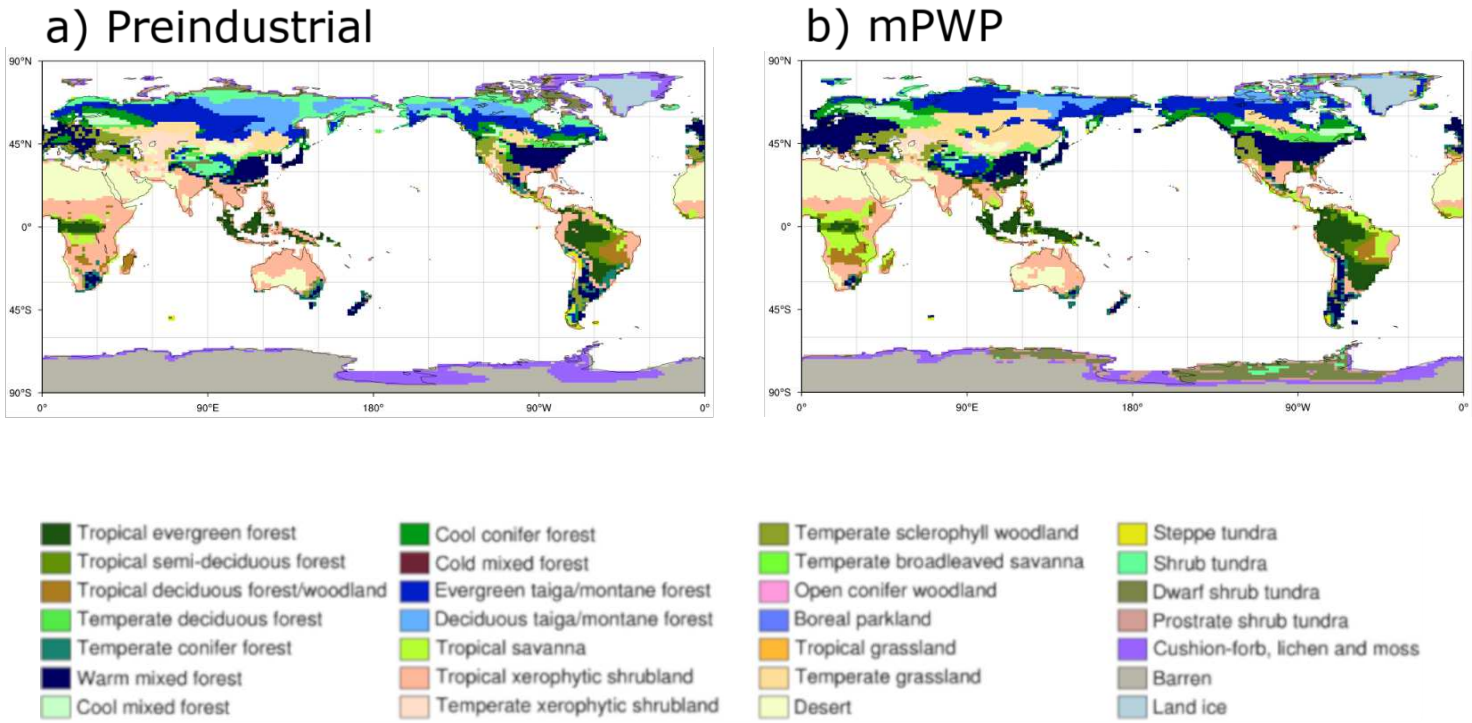

Figure 10: Shows the BIOME4 distribution for the Preindustrial and mPWP

6. Discussion and conclusions

This paper has introduced new simulations of the mPWP carried out with the HadGEM2 model. This model is approximately 20 times slower to run than its predecessor, HadCM3 and is notably more sensitive to the changes in boundary conditions for the mPWP. Because of the slow run time of HadGEM2 it was not feasible to spin up the mPWP simulation from the preindustrial ocean. Instead the mPWP ocean was initialised with a 2°C warmer than preindustrial state, which meant that the TOA radiation imbalance and global ocean temperature drift in the mPWP HadGEM2 simulation was comparable with the preindustrial. Hence the anomalies between the mPWP and the preindustrial simulations are likely to be robust. It is noted that a small drift remains in both the preindustrial and mPWP HadGEM2 experiments, meaning that there could be small changes in some of the results were it possible to continue both these simulations for the tens of thousands of years required to achieve full equilibrium.

The increased sensitivity in HadGEM2 relative to HadCM3 means that HadGEM2 is at the upper end of the PlioMIP1 models, in its prediction of changes in temperature, precipitation and polar (particularly Arctic) amplification. Since PlioMIP1 models underestimated the SST and SAT anomalies seen in proxy reconstructions (Haywood et al., 2013), the increased sensitivity of HadGEM2 relative to HadCM3 is likely more accurate. However, it is noted that the HadGEM2 simulations continue to underestimate the reconstructed SST and SAT anomalies at high latitude sites.

High latitude temperature increases in HadGEM2 (poleward of 60°) averages 8°C in the northern hemisphere and 7°C in the Southern hemisphere. Although the warming is largest in the winter hemisphere, summer hemisphere high latitude warming is sufficient that both the Arctic and Antarctic are almost sea ice free following the summer melt. The winter reduction in Arctic sea ice (in square kilometres) is just as large as in summer, and loss of sea ice near the

coast can lead to stronger continental precipitation.

The high latitude temperature increase leads to a substantial reduction in northern hemisphere permafrost (ground that has been continuously frozen for more than 2 years). Thawing of permafrost is an important climate tipping point, as the release of methane that was trapped in the permafrost can provide a positive feedback on temperature change. We do not include this in our simulation as the tropospheric chemistry scheme is switched off and trace gases are taken to be a fixed model boundary condition. In addition Hopcroft et al. (2017) showed that (for the LGM at least) methane source changes in HadGEM2-ES can be under sensitive.

PlioMIP1 (Haywood et al., 2013) showed that the mPWP-PI precipitation anomaly varied substantially between models. The mPWP was generally a wetter world, however models disagreed on the magnitude of the change. Here we have split our discussion of precipitation change into mid-high latitude precipitation and tropical precipitation. The mid-high latitude precipitation increased in HadGEM2 in all seasons and over both land and ocean, and was broadly related to regions of increased temperature. It is well known from the Clausius-Clapeyron equation that the water holding capacity of the atmosphere increases by about 7% for each 1°C of temperature increase. This holds reasonably well in the HadGEM2 simulations and evaporation increases are strongly related to temperature increase. This was not the case over land in HadCM3, as the evaporation was limited by soil moisture availability hence the warmer temperatures could not always increase evaporation. Therefore, the mid-high latitude land hydrological cycle responds to the mPWP warming in very different ways in the two models. In HadGEM2 there is no sign of a hydrological drought in the Northern Hemisphere, with plenty of additional soil moisture available for re-evaporation and subsequent precipitation. Only in DJF is there a notable shift in high latitude precipitation without a corresponding increase in local evaporation, in DJF the additional precipitation is supplied from the adjacent

oceans where sea ice has been reduced.

Tropical precipitation responds differently to the changing boundary conditions. Over the tropics some regions and seasons get drier while some get wetter. Contrary to expectations for a warm climate we do not see notable changes in the location of the zonal mean ITCZ, although there is approximately 5% more precipitation. This is perhaps because we have presented results from an equilibrium climate, where both the NH and the SH are warmer, the interhemispheric temperature gradient is small, and the position of the thermal equator is approximately the same. Despite this we see larger changes in the ITCZ in certain regions, such as a northward shift in the summer in the Indian Ocean sector - which will intensify the Indian Monsoon. Reasons for the changes in the ITCZ will be the focus of a subsequent paper.

The 405ppmv CO_2 climate we have looked at here appears to have a positive effect on vegetation, with a reduction in barren land (particularly at high latitudes), and an increase in forests. However, the extent of these changes does differ dependent on whether vegetation is predicted using the TRIFFID DGVM or the offline version of BIOME4. Consistent with other diagnostics, vegetation changes in HadGEM2 follows the same pattern as, but are quantitatively enhanced, compared to HadCM3. The warm/wet climate of the mPWP is warmer and wetter in HadGEM2 than in HadCM3, with the result that trees are more able to expand into grassland, while grasses and shrubs can now occupy areas that could not previously support vegetation.

Just like the real world a climate model has an array of positive and negative feedbacks on climate that cannot be fully analysed here. However, we can determine that the climate dynamics and feedbacks associated with a mPWP world are represented more strongly in HadGEM2 compared to some PlioMIP1 models, and in particular compared to a predecessor of HadGEM2 (HadCM3). The simulated HadGEM2 mPWP climate shows larger anomalies to the preindus-

trial, not just in temperature but in a range of other diagnostics including (but not limited to) those discussed in this paper (sea ice, permafrost, precipitation and vegetation response). Whilst making strides forward this result underlines a truism that our understanding of the dynamics of warm worlds in Earth history is model dependent, and ultimately limited by the current understanding of the climate system and the way that knowledge is incorporated into the design and capabilities of different climate and Earth System Models.

The warm world of the mPWP is often discussed as an analogue for near future climate change. This viewpoint can be useful, but it is clearly too simplistic. The simulations provided herein provide alarming indicators of thresholds in the climate system in a 405ppmv CO_2 world that may have already been crossed, including massive sea ice loss and the melting of permafrost. Yet they also provide some source of reassurance of a planet potentially able to support more vegetation, no large increase in areas under the influence of hydrological drought, and no substantial shift of the ITCZ.

However, it must be remembered that these mPWP simulations represent a pristine natural equilibrium climate state. There are no disturbances in these simulations of vegetation from natural (e.g. fires) or anthropogenic sources, and it is likely that the simulated mPWP vegetation patterns can not represent an analogue for the future. Nor can an equilibrium climate as studied here be truly identical to a near future transient climate state. Nonetheless, mPWP simulations provide highly useful indications of a warm world that can be validated against data, in order that we can understand the sensitivity of temperature to greenhouse gas changes, and also the sensitivity of other climate features to the changes in temperature.

Acknowledgements

Research leading to these results has received funding from the European Research Council under the European Union's Seventh Framework Programme (FP7/2007-2013)/ERC grant agreement no. 278636. We would also like to thank Peter Hopcroft and NCAS Computational Modelling Services for help with setting up the HadGEM2 simulations. The HadGEM2 simulations were undertaken on Polaris, part of the N8 High Performance Computing Facilities.

References

Bragg, F.J., Lunt, D.J., Haywood, A.M., 2012. Mid-Pliocene climate modelled using the UK Hadley Centre Model: PlioMIP Experiments 1 and 2. Geosci. Model Dev. 5, 1109–1125. doi:{10.5194/gmd-5-1109-2012}.

Burke, K.D., Williams, J.W., Chandler, M.A., Haywood, A.M., Lunt, D.J., Otto-Bliesner, B.L., 2018. Pliocene and Eocene provide best analogs for near-future climates. P. Natl. Acad. Sci. U.S.A. 115, 13288–13293. doi:{10.1073/pnas.1809600115}.

Chan, W.L., Abe-Ouchi, A., Ohgaito, R., 2011. Simulating the mid-Pliocene climate with the MIROC general circulation model: experimental design and initial results. Geosci. Model Dev. 4, 1035–1049. doi:{10.5194/gmd-4-1035-2011}.

Chandler, M., Rind, D., Thompson, R., 1994. Joint Investigations of the Middle Pliocene Climate .2. GISS GCM Northern-Hemisphere Results. Glob. Planet. Chang. 9, 197–219. doi:{10.1016/0921-8181(94)90016-7}.

Chandler, M.A., Sohl, L.E., Jonas, J.A., Dowsett, H.J., Kelley, M., 2013. Simulations of the mid-Pliocene Warm Period using two versions of the NASA/GISS ModelE2-R Coupled Model. Geosci. Model Dev. 6, 517–531. doi:{10.5194/gmd-6-517-2013}.

Collins, W.J., Bellouin, N., Doutriaux-Boucher, M., Gedney, N., Halloran, P., Hinton, T., Hughes, J., Jones, C.D., Joshi, M., Liddicoat, S., Martin, G., O'Connor, F., Rae, J., Senior, C., Sitch, S., Totterdell, I., Wiltshire, A., Woodward, S., 2011. Development and evaluation of an Earth-System model-HadGEM2. Geosci. Model Dev. 4, 1051–1075. doi:{10.5194/gmd-4-1051-2011}.

Corvec, S., Fletcher, C.G., 2017. Changes to the tropical circulation in the mid-Pliocene and their implications for future climate. Clim. Past 13, 135–147. doi:{10.5194/cp-13-135-2017}.

Cox, P., 2001. Description of the TRIFFID Dynamic Global Vegetation Model. Technical Report 24. UKMO, Hadley Centre.

Dolan, A.M., Haywood, A.M., Hunter, S.J., Tindall, J.C., Dowsett, H.J., Hill, D.J., Pickering, S.J., 2015. Modelling the enigmatic Late Pliocene Glacial Event - Marine Isotope Stage M2. Glob. Planet. Chang. 128, 47–60. doi:{10.1016/j.gloplacha.2015.02.001}.

Dowsett, H., Dolan, A., Rowley, D., Moucha, R., Forte, A.M., Mitrovica, J.X., Pound, M., Salzmann, U., Robinson, M., Chandler, M., Foley, K., Haywood, A., 2016. The PRISM4 (mid-Piacenzian) paleoenvironmental reconstruction. Climate of the Past 12, 1519–1538. doi:{10.5194/cp-12-1519-2016}.

Dowsett, H., Robinson, M., Haywood, A., Salzmann, U., Hill, D., Sohl, L., Chandler, M., Williams, M., Foley, K., Stoll, D., 2010. The PRISM3D paleoenvironmental reconstruction. Stratigraphy 7, 123–139.

Dowsett, H.J., Foley, K.M., Stoll, D.K., Chandler, M.A., Sohl, L.E., Bentsen, M., Otto-Bliesner, B.L., Bragg, F.J., Chan, W.L., Contoux, C., Dolan, A.M., Haywood, A.M., Jonas, J.A., Jost, A., Kamae, Y., Lohmann, G., Lunt, D.J., Nisancioglu, K.H., Abe-Ouchi, A., Ramstein, G., Riesselman, C.R., Robinson, M.M., Rosenbloom, N.A., Salzmann, U., Stepanek, C., Strother, S.L., Ueda, H., Yan, Q., Zhang, Z., 2013. Sea Surface Temperature of the mid-Piacenzian Ocean: A Data-Model Comparison. Scientific Reports 3. doi:{10.1038/srep02013}.

Feng, R., Otto-Bliesner, B.L., Fletcher, T.L., Tabor, C.R., Ballantyne, A.P., Brady, E.C., 2017. Amplified Late Pliocene terrestrial warmth in northern high latitudes from greater radiative forcing and closed Arctic Ocean gateways. Earth. Planet. Sci. Lett. 466, 129–138. doi:{10.1016/j.epsl.2017.03.006}.

Gordon, C., Cooper, C., Senior, C., Banks, H., Gregory, J., Johns, T., Mitchell, J., Wood, R., 2000. The simulation of SST, sea ice extents and ocean heat

transports in a version of the Hadley Centre coupled model without flux adjustments. Clim. Dyn. 16, 147–168.

Haywood, A., Valdes, P., 2004. Modelling Pliocene warmth: contribution of atmosphere, oceans and cryosphere. Earth. Planet. Sci. Lett. 218, 363–377. doi:{10.1016/S0012-821X(03)00685-X}.

Haywood, A., Valdes, P., Sellwood, B., 2002. Magnitude of climate variability during middle Pliocene warmth: a palaeoclimate modelling study. Palaeogeogr. Palaeoclimatol. Palaeoecol. 188, 1–24. doi:{10.1016/S0031-0182(02)00506-0}.

Haywood, A.M., Dolan, A.M., Pickering, S.J., Dowsett, H.J., McClymont, E.L., Prescott, C.L., Salzmann, U., Hill, D.J., Hunter, S.J., Lunt, D.J., Pope, J.O., Valdes, P.J., 2013. On the identification of a Pliocene time slice for data-model comparison. Philos. T. Roy. Soc. A 371. doi:{10.1098/rsta.2012.0515}.

Haywood, A.M., Dowsett, H.J., Dolan, A.M., Rowley, D., Abe-Ouchi, A., Otto-Bliesner, B., Chandler, M.A., Hunter, S.J., Lunt, D.J., Pound, M., Salzmann, U., 2016. The Pliocene Model Intercomparison Project (PlioMIP) Phase 2: scientific objectives and experimental design. Clim. Past 12, 663–675. doi:{10.5194/cp-12-663-2016}.

Haywood, A.M., Dowsett, H.J., Robinson, M.M., Stoll, D.K., Dolan, A.M., Lunt, D.J., Otto-Bliesner, B., Chandler, M.A., 2011. Pliocene Model Intercomparison Project (PlioMIP): experimental design and boundary conditions (Experiment 2). Geosci. Model Dev. 4, 571–577.

Haywood, A.M., Hill, D.J., Dolan, A.M., Otto-Bliesner, B.L., Bragg, F., Chan, W.L., Chandler, M.A., Contoux, C., Dowsett, H.J., Jost, A., Kamae, Y., Lohmann, G., Lunt, D.J., Abe-Ouchi, A., Pickering, S.J., Ramstein, G., Rosenbloom, N.A., Salzmann, U., Sohl, L., Stepanek, C., Ueda, H., Yan, Q., Zhang, Z., 2013. Large-scale features of Pliocene climate: results from the Pliocene Model Intercomparison Project. Clim. Past 9, 191–209.

Haywood, A.M., Valdes, P.J., 2006. Vegetation cover in a warmer world simulated using a dynamic global vegetation model for the Mid-Pliocene. Palaeogeogr. Palaeoclimatol. Palaeoecol. 237, 412–427. doi:{10.1016/j.palaeo.2005.12.012}.

Haywood, A.M., Valdes, P.J., Sellwood, B.W., 2000. Global scale palaeoclimate reconstruction of the middle Pliocene climate using the UKMO GCM: initial results. Glob. Planet. Chang. 25, 239–256.

Hill, D.J., 2015. The non-analogue nature of Pliocene temperature gradients. Earth. Planet. Sci. Lett. 425, 232–241. doi:{10.1016/j.epsl.2015.05.044}.

Hopcroft, P.O., Valdes, P.J., 2015. Last glacial maximum constraints on the Earth System model HadGEM2-ES. Clim. Dyn. 45, 1657–1672. doi:{10.1007/s00382-014-2421-0}.

Hopcroft, P.O., Valdes, P.J., O'Connor, F.M., Kaplan, J.O., Beerling, D.J., 2017. Understanding the glacial methane cycle. Nature Comm. 8. doi:{10.1038/ncomms14383}.

Hunke, E.C., Lipscomb, W.H., 2004. CICE: The Los Alamos Sea Ice Model, documentation and softward, Version 3.1, LA-CC-98-16. Technical Report. Los Alamos National Laboratory, Los Alamos, NM.

Hunter, S.J., Haywood, A.M., Dolan, A.M., Tindall, J.C., 2019. The hadcm3 contribution to pliomip phase 2 part 1: Core and tier 1 experiments. Climate of the Past doi:10.5194/cp-2018-180.

Johns, T., Durman, C., Banks, H., Roberts, M., McLaren, A., Ridley, J., Senior, C., Williams, K., Jones, A., Rickard, G., Cusack, S., Ingram, W., Crucifix, M., Sexton, D., Joshi, M., Dong, B., Spencer, H., Hill, R., Gregory, J., Keen, A., Pardaens, A., Lowe, J., Bodas-Salcedo, A., Stark, S., Searl, Y., 2006. The new Hadley Centre Climate Model (HadGEM1): Evaluation of coupled simulations. J. Clim. 19, 1327–1353. doi:{10.1175/JCLI3712.1}.

Kaplan, J.O., 2001. Geophysical Applications of Vegetation Modeling. Ph.D. thesis. Lund University. Lund.

Lunt, D.J., Huber, M., Anagnostou, E., Baatsen, M.L.J., Caballero, R., DeConto, R., Dijkstra, H.A., Donnadieu, Y., Evans, D., Feng, R., Foster, G.L., Gasson, E., von der Heydt, A.S., Hollis, C.J., Inglis, G.N., Jones, S.M., Kiehl, J., Turner, S.K., Korty, R.L., Kozdon, R., Krishnan, S., Ladant, J.B., Langebroek, P., Lear, C.H., LeGrande, A.N., Littler, K., Markwick, P., Otto-Bliesner, B., Pearson, P., Poulsen, C.J., Salzmann, U., Shields, C., Snell, K., Staerz, M., Super, J., Tabor, C., Tierney, J.E., Tourte, G.J.L., Tripati, A., Upchurch, G.R., Wade, B.S., Wing, S.L., Winguth, A.M.E., Wright, N.M., Zachos, J.C., Zeebe, R.E., 2017. The DeepMIP contribution to PMIP4: experimental design for model simulations of the EECO, PETM, and pre-PETM (version 1.0). Geosci. Model Dev. 10, 889–901. doi:{10.5194/gmd-10-889-2017}.

Martin, G., Ringer, M., Pope, V., Jones, A., Dearden, C., Hinton, T., 2006. The physical properties of the atmosphere in the new Hadley Centre Global Environmental Model (HadGEM1). Part I: Model description and global climatology. J. Clim. 19, 1274–1301. doi:{10.1175/JCLI3636.1}.

Martin, G.M., Milton, S.F., Senior, C.A., Brooks, M.E., Ineson, S., Reichler, T., Kim, J., 2010. Analysis and Reduction of Systematic Errors through a Seamless Approach to Modeling Weather and Climate. J. Clim. 23, 5933–5957. doi:{10.1175/2010JCLI3541.1}.

Otto-Bliesner, B.L., Braconnot, P., Harrison, S.P., Lunt, D.J., Abe-Ouchi, A., Albani, S., Bartlein, P.J., Capron, E., Carlson, A.E., Dutton, A., Fischer, H., Goelzer, H., Govin, A., Haywood, A., Joos, F., LeGrande, A.N., Lipscomb, W.H., Lohmann, G., Mahowald, N., Nehrbass-Ahles, C., Pausata, F.S.R., Peterschmitt, J.Y., Phipps, S.J., Renssen, H., Zhang, Q., 2017. The PMIP4 contribution to CMIP6-Part 2: Two interglacials, scientific objective and ex-

perimental design for Holocene and Last Interglacial simulations. Geosci. Model Dev. 10, 3979–4003. doi:{10.5194/gmd-10-3979-2017}.

Pope, V., Gallani, M., Rowntree, P., Stratton, R., 2000. The impact of new physical parametrizations in the Hadley Centre climate model: HadAM3. Clim. Dyn. 16, 123–146.

Pound, M.J., Tindall, J., Pickering, S.J., Haywood, A.M., Dowsett, H.J., Salzmann, U., 2014. Late Pliocene lakes and soils: a global data set for the analysis of climate feedbacks in a warmer world. Clim. Past 10, 167–180. doi:{10.5194/cp-10-167-2014}.

Prescott, C.L., Dolan, A.M., Haywood, A.M., Hunter, S.J., Tindall, J.C., 2018. Regional climate and vegetation response to orbital forcing within the mid-Pliocene Warm Period: A study using HadCM3. Glob. Planet. Chang. 161, 231–243. doi:{10.1016/j.gloplacha.2017.12.015}.

Salzmann, U., Dolan, A.M., Haywood, A.M., Chan, W.L., Voss, J., Hill, D.J., Abe-Ouchi, A., Otto-Bliesner, B., Bragg, F.J., Chandler, M.A., Contoux, C., Dowsett, H.J., Jost, A., Kamae, Y., Lohmann, G., Lunt, D.J., Pickering, S.J., Pound, M.J., Ramstein, G., Rosenbloom, N.A., Sohl, L., Stepanek, C., Ueda, H., Zhang, Z.S., 2013. Challenges in quantifying Pliocene terrestrial warming revealed by data-model discord. Nat. Clim. Chang. 3, 969–974.

Salzmann, U., Haywood, A.M., Lunt, D.J., Valdes, P.J., Hill, D.J., 2008. A new global biome reconstruction and data-model comparison for the Middle Pliocene. Global Ecol. Biogeogr. 17, 432–447.

Screen, J.A., Simmonds, I., 2010. The central role of diminishing sea ice in recent Arctic temperature amplification. Nature 464, 1334–1337. doi:{10.1038/nature09051}.

Sloan, L., Crowley, T., Pollard, D., 1996. Modeling of middle pliocene climate with the NCAR GENESIS general circulation model. Marine Micropaleontology 27, 51–61. doi:{10.1016/0377-8398(95)00063-1}.

Solomon, S., Qin, D., Manning, M., Z. Chen, a.M.M., Averyt, K.B., Tignor, M., Miller, H.L. (Eds.), 2007. IPCC, 2007 Climate Change 2007: The Physical Science Basis. Contribution of Working Group I to the Fourth Assessment Report of the Intergovernmental Panel on Climate Change. Cambridge University Press, Cambridge, United Kingdom and New York, NY, USA.

Stepanek, C., Lohmann, G., 2012. Modelling mid-Pliocene climate with COSMOS. Geosci. Model Dev. 5, 1221–1243. doi:{10.5194/gmd-5-1221-2012}.

Stocker, T.F., Qin, D., Plattner, G.K., Tignor, M., Allen, S.K., Boschung, J., Nauels, A., Xia, Y., Bex, V., Midgley, P.M. (Eds.), 2013. IPCC, 2013 Climate Change 2013: The Physical Science Basis. Contribution of Working Group I to the Fifth Assessment Report of the Intergovernmental Panel on Climate Change. Cambridge University Press, Cambridge, United Kingdom and New York, NY, USA.

Taylor, K.E., Crucifix, M., Braconnot, P., Hewitt, C.D., Doutriaux, C., Broccoli, A.J., Mitchell, J.F.B., Webb, M.J., 2007. Estimating shortwave radiative forcing and response in climate models. J. Clim. 20, 2530–2543. doi:{10.1175/JCLI4143.1}.

Taylor, K.E., Stouffer, R.J., Meehl, G.A., 2012. AN OVERVIEW OF CMIP5 AND THE EXPERIMENT DESIGN. B. Am. Meteorol. Soc. 93, 485–498. doi:{10.1175/BAMS-D-11-00094.1}.

The HadGEM2 Dev Team, 2011. The HadGEM2 family of Met Office Unified Model climate configurations. Geosci. Model Dev. 4, 723–757. doi:{10.5194/gmd-4-723-2011}.

Tindall, J.C., Haywood, A.M., 2015. Modeling oxygen isotopes in the Pliocene: Large-scale features over the land and ocean. Paleoceanography 30, 1183–1201. doi:{10.1002/2014PA002774}.

Tindall, J.C., Haywood, A.M., Howell, F.W., 2016. Accounting for centennial-

scale variability when detecting changes in ENSO: A study of the Pliocene. Paleoceanography 31, 1330–1349. doi:{10.1002/2016PA002951}.

Unger, N., Yue, X., 2014. Strong chemistry- climate feedbacks in the Pliocene. Geophys. Res. Lett. 41, 527–533. doi:{10.1002/2013GL058773}.

Valdes, P.J., Armstrong, E., Badger, M.P.S., Bradshaw, C.D., Bragg, F., Crucifix, M., Davies-Barnard, T., Day, J.J., Farnsworth, A., Gordon, C., Hopcroft, P.O., Kennedy, A.T., Lord, N.S., Lunt, D.J., Marzocchi, A., Parry, L.M., Pope, V., Roberts, W.H.G., Stone, E.J., Tourte, G.J.L., Williams, J.H.T., 2017. The BRIDGE HadCM3 family of climate models: HadCM3@Bristol v1.0. Geosci. Model Dev. 10, 3715–3743. doi:{10.5194/gmd-10-3715-2017}.

Zhang, Z.S., Nisancioglu, K.H., Chandler, M.A., Haywood, A.M., Otto-Bliesner, B.L., Ramstein, G., Stepanek, C., Abe-Ouchi, A., Chan, W.L., Bragg, F.J., Contoux, C., Dolan, A.M., Hill, D.J., Jost, A., Kamae, Y., Lohmann, G., Lunt, D.J., Rosenbloom, N.A., Sohl, L.E., Ueda, H., 2013. Mid-pliocene Atlantic Meridional Overturning Circulation not unlike modern. CLIMATE OF THE PAST 9, 1495–1504. doi:{10.5194/cp-9-1495-2013}.

Zheng, W., Zhang, Z., Chen, L., Yu, Y., 2013. The mid-Pliocene climate simulated by FGOALS-g2. Geosci. Model Dev. 6, 1127–1135. doi:{10.5194/gmd-6-1127-2013}.